Asian Journal of Pharmaceutical Sciences 16 (2021) 784–793

Available online at www.sciencedirect.com

ScienceDirect

journal homepage: www.elsevier.com/locate/AJPS

Original Research Paper

Iron-doxorubicin prodrug loaded liposome nanogenerator programs multimodal ferroptosis for efficient cancer therapy

Yinxian Yang[a], *Shiyi Zuo*[b], *Linxiao Li*[b], *Xiao Kuang*[b], *Jinbo Li*[b], *Bingjun Sun*[b,*], *Shujun Wang*[a,*], *Zhonggui He*[b], *Jin Sun*[b,*]

[a] *Department of Pharmaceutics, College of Pharmacy, Shenyang Pharmaceutical University, Shenyang 110016, China*
[b] *Department of Pharmaceutics, Wuya College of Innovation, Shenyang Pharmaceutical University, Shenyang 110016, China*

ARTICLE INFO

Article history:
Received 10 February 2021
Revised 1 April 2021
Accepted 24 May 2021
Available online 6 June 2021

Keywords:
Ferroptosis
Iron
Liposome
Redox
Prodrug

ABSTRACT

Ferroptosis is a new mode of cell death, which can be induced by Fenton reaction-mediated lipid peroxidation. However, the insufficient H_2O_2 and high GSH in tumor cells restrict the efficiency of Fenton reaction-dependent ferroptosis. Herein, a self-supplying lipid peroxide nanoreactor was developed to co-delivery of doxorubicin (DOX), iron and unsaturated lipid for efficient ferroptosis. By leveraging the coordination effect between DOX and Fe^{3+}, trisulfide bond-bridged DOX dimeric prodrug was actively loaded into the core of the unsaturated lipids-rich liposome via iron ion gradient method. First, Fe^{3+}could react with the overexpressed GSH in tumor cells, inducing the GSH depletion and Fe^{2+}generation. Second, the cleavage of trisulfide bond could also consume GSH, and the released DOX induces the generation of H_2O_2, which would react with the generated Fe^{2+}in step one to induce efficient Fenton reaction-dependent ferroptosis. Third, the formed Fe^{3+}/Fe^{2+} couple could directly catalyze peroxidation of unsaturated lipids to boost Fenton reaction-independent ferroptosis. This iron-prodrug liposome nanoreactor precisely programs multimodal ferroptosis by integrating GSH depletion, ROS generation and lipid peroxidation, providing new sights for efficient cancer therapy.

1. Introduction

Cancer remains one of the leading causes of death over the world [1]. Triggering tumor cell death through apoptosis-mediated pathways is one of the principal approaches for cancer therapy, whereas the increasing drug resistance greatly restricts the efficacy of apoptosis [2–6]. The development of novel cell death pathways shows potential to overcome these obstructs. Ferroptosis is recognized as a new type of cell death, which is a quite distinct from apoptosis [7,8]. Emerging evidence shows ferroptosis is induced by iron-dependent lipid peroxide accumulations [7,9]. Typically, ferroptosis is often initiated by Fenton chemistry, in which Fe^{2+} could

* Corresponding authors.
E-mail addresses: sunbingjun@aliyun.com (B. Sun), 101030124@syphu.edu.cn (S. Wang), sunjin@syphu.edu.cn (J. Sun).
Peer review under responsibility of Shenyang Pharmaceutical University.
https://doi.org/10.1016/j.ajps.2021.05.001

react with H_2O_2 to generate hydroxyl radicals, and then triggering the oxidation of unsaturated lipids [9,10]. Up to now, various iron-nanomaterials have been developed to increase intracellular iron to trigger ferroptosis in tumor cells [10,11]. Nevertheless, high GSH and insufficient H_2O_2 in tumors often restrict the iron-mediated hydroxyl radical production, subsequently compromising the Fenton reaction-dependent ferroptosis [11,12].

Fortunately, iron could also cause ferroptosis via other pathways expect for Fenton chemistry, such as iron redox couple-catalyzed oxidation of unsaturated lipids [9,13–15]. Several studies have reported iron-induced oxidation in liposomes and iron loaded liposome triggered lipid peroxide for ferroptosis therapy [15–17]. It is noteworthy that the co-exist of Fe^{3+} and Fe^{2+} is required for iron-induced oxidation of unsaturated lipid in the absence H_2O_2 [15,16]. Therefore, the co-delivery of Fe^{3+} and unsaturated lipid is promising to trigger lipid peroxidation for ferroptosis. In tumor cells, Fe^{3+} could react with intracellular GSH, result in GSH depletion and reduce $Fe^{3+}$to Fe^{2+}. Subsequently, the formed Fe^{3+}/Fe^{2+}couple could directly catalyze oxidation of unsaturated lipid for Fenton-independent ferroptosis [16]. Meanwhile, the Fe^{2+}could further react with H_2O_2 to produce hydroxyl radical via Fenton chemistry, which induces Fenton-dependent ferroptosis [11,18]. Altogether, it is promising to induce efficient ferroptosis via two primary pathways: (i) triggering Fenton-independent ferroptosis by providing Fe^{3+}/Fe^{2+}couple and unsaturated lipid; (ii) inducing Fenton-dependent ferroptosis by the increase of $Fe^{2+}$and H_2O_2 supply in tumor cells

It is reported that DOX could produce H_2O_2 to amplify the ferroptosis effects of iron by activating the NADPH oxidase 4 (NOX4) in tumor cells [19]. Nevertheless, free DOX often induces serious adverse effects, such as cardio toxicity and dose-limiting myelosuppression [20]. Doxil (liposomal DOX), significantly increases the circulation time but reduces cardiomyopathy compared with free DOX [21]. However, owing to its extremely long circulation time, the high accumulation of DOX in skin results in severe hand-foot syndrome [21]. Therefore, efforts have been devoted to improve safety of long-circulating liposomes, including enhancing the targeting ability of liposomes or loaded molecules [22–24]. Stimuli-responsive prodrug can be activated in response to tumor microenvironment, allowing selective drug release in tumors and reduced non-specific toxicity in normal tissues [25–27]. Typically, our group previously developed a series of redox-responsive prodrug nanoassemblies for anticancer drug self-delivery due to the high redox heterogeneity in tumor cells [28–30]. Despite its excellent redox-responsiveness and improved assembly ability, trisulfide bond-bridged DOX dimeric prodrug nanoassemblies still seriously suffer from rapid blood clearance [28]. To improve the delivery efficiency and stability, prodrugs with special structure are capable to be loaded into liposome interior [23,31]. Notably, DOX could be loaded into inner core of liposomes via Mn^{2+} or Cu^{2+} gradient method by the formation of metal-DOX coordinated complex [23,32]. Therefore, we speculate that DOX dimeric prodrug could also coordinate with Fe^{3+}, and then be actively loaded into iron liposome by iron ion gradient method.

On the basic of the above findings, we developed a self-supplying lipid peroxide nanogenerator by co-delivery of DOX, iron and unsaturated lipid for efficient ferroptosis (Fig. 1A). In brief, a GSH-responsive trisulfide bond-bridged DOX homodimeric prodrug (DSSSD) was actively loaded into the core of the unsaturated lipids-rich liposome via iron ion gradient method. The Fe^{3+} not only allows for efficient loading of prodrug by leveraging the coordination effect between DOX and Fe^{3+}, but also provides iron-based multimodal ferroptosis therapy. First, the reaction of Fe^{3+} with intracellular GSH could induce GSH depletion and produce Fe^{2+} to catalyze Fenton reaction (Fig. 1B). Second, the cleavage of trisulfide bond could also consume GSH and the released DOX enhances the generation of H2O2 by up-regulation of NOX4, subsequently amplifying the Fe^{2+}-mediated Fenton reaction-dependent ferroptosis. Third, the formed Fe^{3+}/Fe^{2+} redox couple could directly trigger unsaturated lipids-rich liposomes into lipid peroxide for Fenton reaction-independent ferroptosis. Compared with other Fenton-dependent ferroptosis strategies, the developed iron-prodrug loaded liposome is anticipated to induce ferroptosis through multiple pathways, including Fenton-dependent hydroxyl radical generation, Fenton-independent lipid peroxide production and GSH depletion (Fig. 1B).

2. Materials and methods

2.1. Materials

Doxorubicin hydrochloride, MTT and DiR were supplied by Meilun Biotech Co. Ltd. (Dalian, China). 1,2-distearoyl-sn–glycero-3-phosphoethanolamine-N-[amino(polyethyleneglycol)−2000] (DSPE-PEG2k), phosphatidylcholine (PC) and cholesterol were purchased from Shanghai Advanced Vehicle Technology Pharmaceutical Ltd., (Shanghai, China). Ferric ammonium citrate and ethylenediamine tetraacetic acid (EDTA) were obtained from Yuwang Pharm. (Shandong, China). GSH were offered by Aladdin (Shanghai, China). C11-BODIPY 581/591 were purchased from Maokang Biotechnology (Shanghai, China). ROS Assay Kit and GSH Assay Kit were offered by Beyotime (Shanghai, China). Sepharose CL-4B gel, hydroxyethyl piperazine ethylsulfonic acid (HEPES) and Hoechst 33,342 was provided by Solarbio Science and Technology Co. Ltd. (Beijing, China). 96-well plates were purchased from NEST Biotechnology (Wuxi, China). Fetal bovine serum (FBS) was obtained from Hyclone (Beijing, China).

2.2. Preparation and characterization of liposomes

2.2.1. Synthesis of DOX prodrugs

The detailed synthesis method for DOX dimeric prodrugs has been reported in published literature [28].

2.2.2. Preparation of liposomes

Briefly, PC: DSPE-PEG2k: cholesterol (90:10:10) were dissolved in chloroform, and then removed chloroform through rotary evaporation at 37 °C. The obtained lipid thin film was hydrated with 250 mM ferric ammonium citrate at 60 °C for 1 h, and

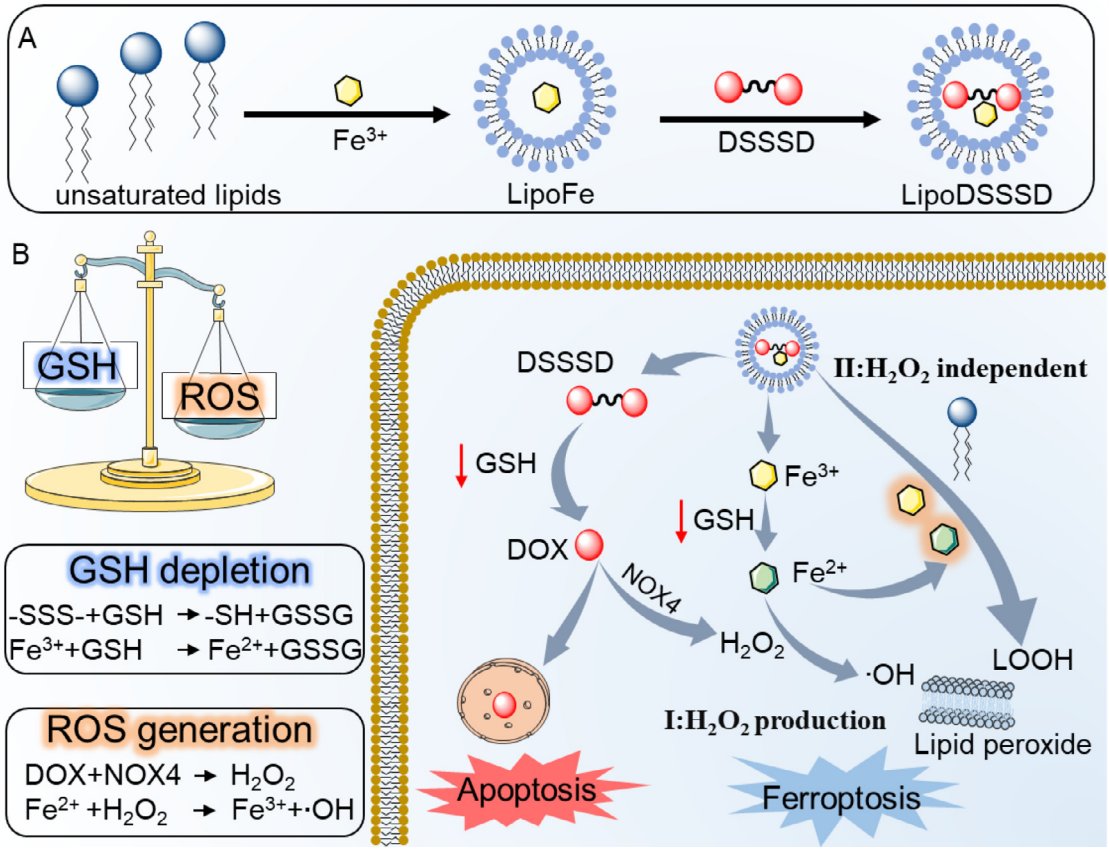

Fig. 1 – (A) Illustration of the synthesis of Fe^{3+}-prodrug loaded liposome. (B) Schematic of GSH-responsive multiple functional liposome-augmented synergistic ferroptosis and apoptosis for cancer therapy. On one hand, the reaction of Fe^{3+} with intracellular GSH could produce Fe^{2+} to catalyze Fenton reaction while released DOX further produce H_2O_2 to amplify Fenton-mediated ferroptosis. On the other hand, the formed Fe^{3+}/Fe^{2+} redox couple could directly trigger unsaturated lipids-rich liposomes into lipid hydroperoxide for Fenton-independent ferroptosis. LOOH, lipid hydroperoxide; -SSS-, trisulfide bond; DSSSD, trisulfide bond-bridged DOX prodrugs; LipoFe, Fe^{3+} loaded liposomes; LipoDSSSD, DSSSD-Fe^{3+} loaded liposomes; NOX4, NADPH oxidase 4.

then sonicated for 10 min to get blank liposome (LipoFe). The unencapsulated Fe^{3+} was removed by elution with HEPES and EDTA buffer on a gel column. The water insoluble DOX prodrugs were loaded in liposomal interior by solvent-assisted active loading technology. In brief, prodrugs were dissolved in DMSO and added to iron liposome with stirring at 60 °C for 60 min. Unencapsulated drugs and the residual organic solvent were removed through a gel column using HEPES buffered saline.

2.2.3. *Characterization of liposomes*

The dynamic diameter and zeta potential were measured by the Zetasizer Nano ZS90 instrument (Nano ZS, Malvern Co., UK). TEM was used to observed the morphology of formulations. The encapsulation efficiency (EE%) and drug loading (DL%) was measured by HPLC (Hitachi). Chromatographic separation was achieved on an Ultimate@XB-C18 column (4.6 mm × 150 mm, 5 μm) (Welch, Shanghai, China) at the ultraviolet wavelength of 232 nm. The mobile phase consisted of methanol and water (70:30) at a flow rate of 1.0 ml/min. Colloidal stability of the liposomes was investigated in PBS containing 10% of FBS at 37 °C, and the hydrodynamic diameter was monitored during the time.

2.2.4. *In vitro drug release*

GSH-triggered drug release of LipoDSSSD was tested in the different concentration of GSH. First, the fluorescence of DOX and prodrugs were investigated using a microplate reader. Then, LipoDSSSD was incubated with PBS (pH 7.4) containing 10% ethanol (v/v) with or without GSH at 37 °C. The 50 μl samples were collected and added into 200 μl of methanol for the fluorescence measurement (λ_{ex} = 480 nm, λ_{em} = 580 nm) at different time points.

2.3. *Cytotoxicity and cellular uptake*

B16-F10 melanoma cells were seeded in 96-well plates (2500 cells/well) and cultured overnight. The cells were incubated with corresponding formulations diluted with culture medium in different concentrations for 24 h, Then, cells were incubated with 20 μl MTT (5 μg/ml) for another

4 h. The formed formazan crystals were dissolved in DMSO, and the absorbance was recorded at 490 nm. For cellular uptake, B16-F10 cells (1×10^5 cells/well) were seeded on coverslips overnight. Then, cells were incubated with DOX and LipoDSSSD at the concentration of 5 μg/ml. After 6 h and 12 h, the cells were washed, fixed and stained with Hoechst 33,342. The fluorescent images were observed by CLSM. To quantify the cellular uptake, the cells were collected in PBS after treatment for flow cytometry analysis on a FACSCalibur instrument.

2.4. Intracellular ROS, GSH and lipid peroxide assay

B16-F10 cells were seeded overnight and treated with various formulations at an equivalent level for 24 h. Then, ROS and GSH level was measured using a ROS or GSH Assay kit. Briefly, after treatment for 24 h, the cells were incubated with DCFH-DA (10 μM) for 30 min. After that, the cells were washed and observed by CLSM. For qualitative analysis of ROS fluorescence, cells were seeded and treated as the aforementioned protocols. Then, cells were collected for flow cytometry analysis. For GSH assay, GSH level was measured by a microplate reader following the manufacturer's instruction. For lipid peroxide assay, the cells were washed and incubated with C11-BODIPY 581/591 (10 μM) for 30 min. The fluorescent of treated cells was observed by CLSM.

2.5. Pharmacokinetics

For pharmacokinetics study, LipoDSSSD (2 mg/kg equivalent DOX) or free DOX (2 mg/kg) were intravenously injected into the male SD rats ($n = 3$). Then, blood samples were obtained and centrifuged at 13 000 rpm for 10 min to separate the plasma. The obtained samples were analyzed by UPLC-MS/MS on an ACQUITY UPLC system (Waters, Milford, MA, USA).

2.6. In vivo biodistribution

The biodistribution was investigated in B16-F10 melanoma bearing mice. When the tumor volume reached about 500 mm^3, DiR solution and DiR labeled liposomes were administered intravenously at a dose equivalent of 2 mg/kg. After administration for 4, 12 and 24 h, mice were sacrificed. The major organs and tumors were collected for *ex vivo* imaging by Caliper IVIS (Perkin Elmer, USA).

2.7. In vivo efficacy and safety

The anticancer efficacy was evaluated in B16-F10 melanoma bearing mice. For the B16-F10 model, B16-F10 cells (5×10^6 cells) were subcutaneously injected into the right flank of female C57BL/6 mice. When the tumors reached an volume of 250 mm^3, mice were intravenously injected with Saline, LipoFe, free DOX, Doxil or LipoDSSSD at an DOX dose of 3 mg/kg every two days for total four times. The tumor volume was monitored and calculated as (tumor length) × (tumor width)^2/2. After treatment, the mice were sacrificed. Plasma was collected for hepatorenal function analysis, and the major organs (hearts, livers, spleens, lungs, and kidneys) were stained with H&E for the histological evaluation. In addition, the tumors were stained using H&E and TUNEL to evaluate the apoptosis levels.

2.8. Statistics

Data analysis were performed using GraphPad Prism 8 and presented as the mean value ± SD. Statistical analysis was performed using Student's *t*-test (two-tailed) and one-way analysis of variance (ANOVA). $P < 0.05$ was considered statistically significant.

3. Results and discussion

3.1. Synthesis of iron-prodrug loaded liposomes

3.1.1. Synthesis of DOX dimeric prodrugs

It is reported that iron could potentiate the efficacy of DOX, while DOX could amplify the ferroptosis effects of iron by producing H_2O_2 [19]. As shown in Fig. S1, trisulfide bond-bridged DOX dimeric prodrugs (DSSSD) was chosen as the model drug over DOX because of its higher tumor selective cytotoxicity [28]. In addition, compared to the conventional disulfide bond, trisulfide bond could react with GSH through the three sulfur atoms, resulting in higher GSH-sensitivity and GSH depletion [32].

3.1.2. Preparation and characterization of liposomes

Iron can catalyze the oxidation of unsaturated lipids to induce ferroptosis [15,16]. To develop a lipid peroxide nanogenerator (Fig. 2A), liposome (LipoFe) was constructed by unsaturated lipids-rich phosphatidylcholine, and Fe^{3+} was encapsulated into the inner core by thin-film hydration method. LipoFe exhibited light yellow appearance (Fig. 2B) and obvious Tyndall effect (Fig. S2). LipoFe showed hydrodynamic diameters of 103.43 ± 0.57 nm and zeta potential of −18.33 ± 1.13 mV (Fig. 2C). TEM images also demonstrated the spheroidal nanostructure of LipoFe (Fig. S3). It is reported that iron liposomes could induce peroxidation of unsaturated lipids, and the co-existing of $Fe^{3+}$and Fe^{2+} is required to initiate oxidation [15,16]. In order to obtain $Fe^{3+}$and Fe^{2+}couple, GSH was added to LipoFe as a reduction agent. Then, the products of lipid oxidation were monitored by mass spectrum. In the presence of GSH, obvious lipid hydroperoxides (LOOH) were observed (*m/z*, 814), compared to the unsaturated lipids (*m/z*, 782) without the addition of GSH (Fig. S4). Therefore, LipoFe could induce oxidation of unsaturated lipid in the presence of GSH, in agreement with previous studies [16,33].

Typically, DOX could be actively loaded into liposome interior by ammonium sulfate (pH) gradient due to the amino protonation of DOX molecule in weakly acidic solution (Fig. S5). However, DSSSD was extremely hydrophobic and failed to be stably loaded into liposome by pH gradient due to the covered amino group (Fig. S6). Alternatively, it is reported that iron and DOX could form a coordination drug-metal complex, which allows for efficient drug loading of DOX [19]. The coordination between Fe^{3+} and DOX could quench the fluorescence of DOX. Therefore, the fluorescence properties of DOX and DSSSD were investigated.

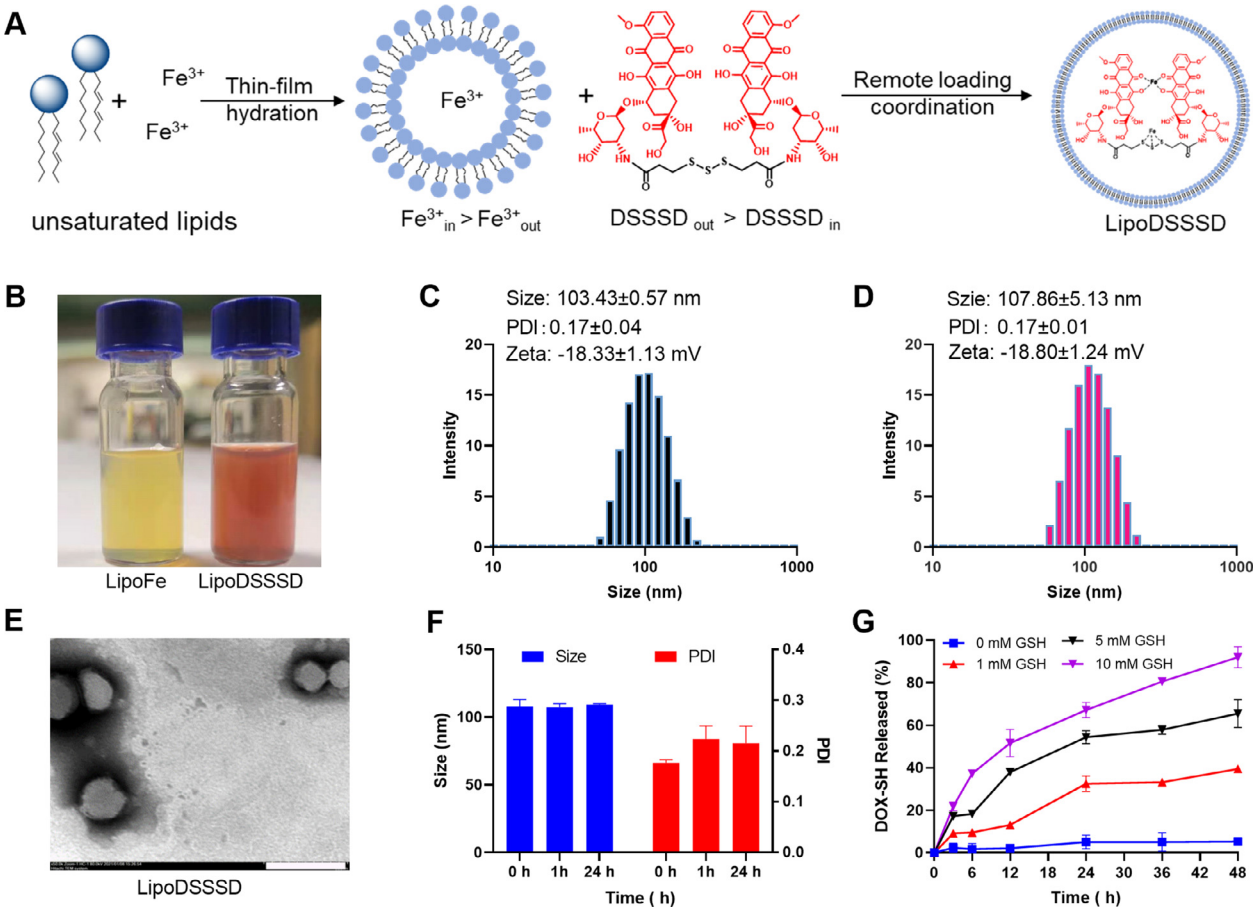

Fig. 2 – Preparation and characterization of the LipoDSSSD. (A) Preparation of LipoFe by thin-film hydration method and remote loading DSSSD into LipoFe by iron ion gradient method. (B) The appearance of LipoFe and LipoDSSSD. (C) The DLS results of LipoFe. (D) The DLS results of LipoDSSSD. (E) TEM image of LipoDSSSD. The scale bar is 200 nm. (F) The colloidal stability of LipoDSSSD in PBS containing 10% FBS (v/v) at 37 °C. (G) GSH-triggered drug release of LipoDSSSD in PBS containing different containing of GSH ($n = 3$).

DSSSD prodrugs showed a significant decreased fluorescence emission compared with DOX (Fig. S7), in accordance with previous studies [28,34]. After incubation with Fe^{3+}, fluorescence of DSSSD was further quenched as same as DOX (Fig. S8), which indicated the formation of DSSSD-Fe^{3+} coordination complex due to its similar structure with DOX. Therefore, DSSSD was encapsulated into the aqueous core of the liposome by the Fe^{3+} gradient between the inside and outside of LipoFe (Fig. 2A). As shown in Fig. S9, a distinct color change was observed from yellow to red to brown during drug loading, indicating the formation of DSSSD and Fe^{3+}coordination complex. Furthermore, TEM image and dynamic light scattering analyses showed that LipoDSSSD exhibited uniform spherical structure with an average diameter of 107.86 ± 5.13 nm (Fig. 2D & 2E). The encapsulate efficiency for DSSSD was approximately 87% ± 5% and the final drug loading of DOX in LipoDSSSD was 7.56%. LipoDSSSD exhibited similar particle size and zeta potential with LipoFe, which could be ascribed to that DSSSD was loaded into inner core of liposomes without disruption of the surface properties of LipoFe. The colloidal stability of liposomes was further evaluated in PBS (pH 7.4) containing 10% fetal bovine serum at 37 °C. LipoDSSSD showed superior colloidal stability with negligible changes in particle size within 24 h (Fig. 2F).

3.1.3. *In vitro drug release*

Next, we examined the drug release of LipoDSSSD, which was a crucial feature for antitumor efficiency and safety. As shown in Fig. S10, the cleavage of the trisulfide bond by GSH can restore the fluorescence of DOX, and DSSSD exhibited GSH-dependent fluorescence recovery. This is due to the released DOX-SH from DSSSD exhibits same fluorescence properties with DOX [28]. As shown in Fig. 2G, about 30% drug was released from LipoDSSSD in the present of 1 mM GSH in compared to 60% for 5 mM GSH. Notably, more than 90% drug was released from LipoDSSSD in the presence of 10 mM GSH (Fig. 2G), suggesting that the efficient prodrug activation is possible in tumor cells due to the high GSH levels. In contrast, few drugs were released from LipoDSSSD in PBS without GSH, in agreement with previous study [28].

3.2. *Cytotoxicity and cellular uptake*

The *in vitro* antitumor activity of LipoFe and LipoDSSSD was investigated in B16-F10 cells. First, we tried to verify whether

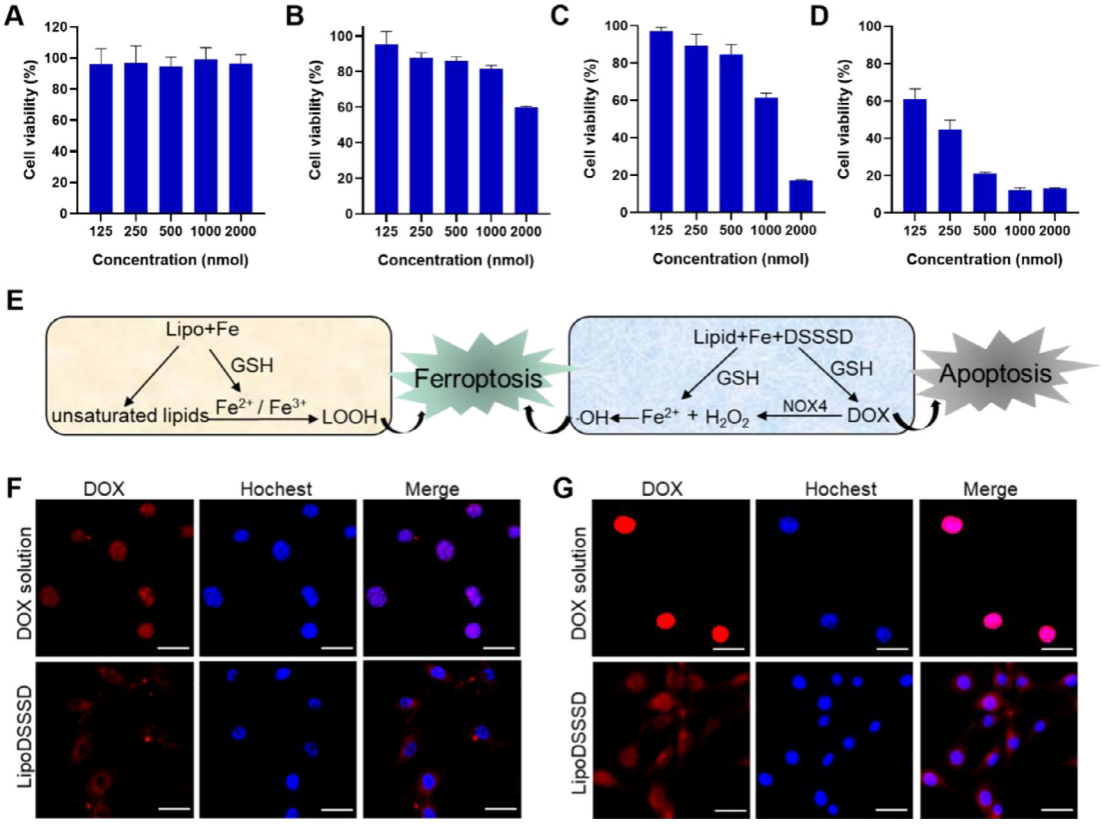

Fig. 3 – Cytotoxicity and cellular uptake of LipoDSSSD in B16-F10 cells. Cell viability of B16-F10 cells incubated with (A) lipid, (B) LipoFe, (C) LipoDSSSD and (D) DOX solution at different concentrations ($n = 3$). The concentration of lipids or liposomes is equivalent to that of LipoDSSSD. (E) The mechanism of cytotoxicity of LipoFe and LipoDSSSD in tumor cells. CLSM image of B16-F10 cells incubated with DOX and LipoDSSSD for (F) 12 h and (G) 24 h. Scale bar represents 20 μm.

lipids impact cell viability. As shown in Fig. 3A, lipids had no effect on cell survival after treatment for 24 h. In comparison, LipoFe showed obvious dose-dependent cytotoxicity on B16-F10 cells (Fig. 3B). The possible mechanism of cytotoxicity for LipoFe was due to the following two aspects (Fig. 3E). On one hand, high GSH level in tumor cells could reduce Fe^{3+} to Fe^{2+} for mild Fenton-dependent ferroptosis. Because insufficient H_2O_2 in tumor cells often restrict the generation of hydroxyl radical, leading to poor Fenton-dependent ferroptosis [12]. On the other hand, the formed iron redox couple (Fe^{3+}/Fe^{2+}) could also directly induce peroxidation of unsaturated lipid for Fenton-independent ferroptosis (Fig. S4). After drug loading, LipoDSSSD exhibited stronger cytotoxicity than LipoFe (Fig. 3C), which could be attributed to following three points. (i) First, the cleavage of trisulfide bond could consume GSH, and the released DOX would intercalate into DNA inducing cell apoptosis. (ii) Second, Fe^{3+} could react with GSH to induce GSH depletion and produce Fe^{2+}. Owing to the activated NOX4 by DOX, the improved H_2O_2 could react with the generated Fe^{2+} for efficient Fenton-dependent ferroptosis. (iii) Third, the formed Fe^{3+}/Fe^{2+} redox couple could directly trigger lipid peroxide of unsaturated lipids-rich liposomes for Fenton-independent ferroptosis. Compared with DOX solution (Fig. 3D), LipoDSSSD exhibited lower cytotoxicity on tumor cells due to the delayed drug release from prodrugs and liposomes. Furthermore, LipoDSSSD exhibited poor cytotoxicity on L02 cells (Fig. S11), indicating its good selectivity between tumor cells and normal cells. This was probably due to that low GSH in normal cells could not effectively reduce Fe^{3+} to Fe^{2+}, and then compromised lipid peroxidation [16]. In addition, the low concentration of intracellular GSH also restricted the cleavage of the trisulfide bond and sequentially reduced the cytotoxicity of DSSSD [28]. Accordingly, LipoDSSSD could selectively kill tumor cells through iron-induced ferroptosis and GSH-induced apoptosis of DSSSD in tumor cells but keep good safety for normal cells (Fig. 3E).

We further investigated the cell uptake of LipoDSSSD in B16-F10 cells. A time-dependent increase in fluorescence intensity was observed when the cells were treated with free DOX or LipoDSSSD (Fig. 3F,G). At the first 12 h, poor fluorescence recovery was observed for LipoDSSSD, with major localization in the cytoplasm. This could attribute to the delayed drug release from LipoDSSSD (Fig. S10). After internalization into tumor cells, the fluorescence of LipoDSSSD gradually increased due to the GSH-triggered drug release in tumor cells, in agreement with *in vitro* drug release (Fig. 2G). When the cells incubated with LipoDSSSD for 24 h, a moderate red fluorescence (DOX) started to colocalize with blue fluorescence (cell nucleus), indicating its efficient migration from cytoplasm to the nucleus. These results demonstrated that the cleavage of

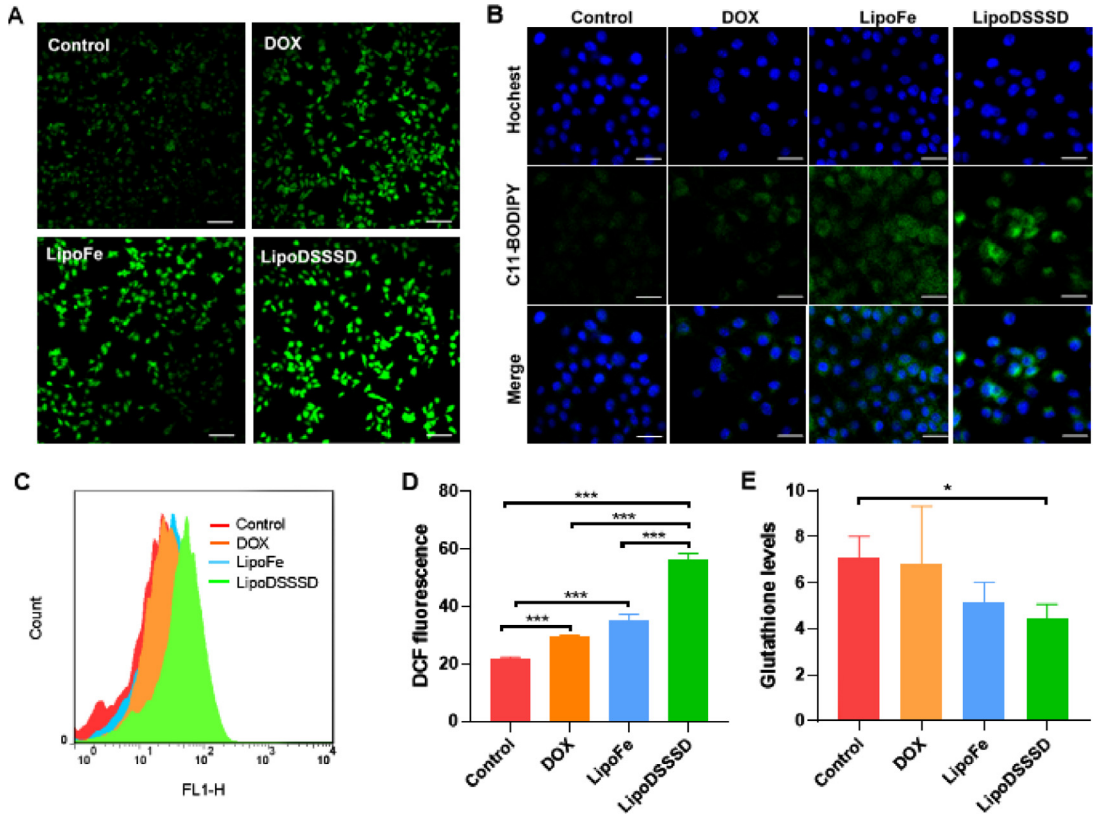

Fig. 4 – Intracellular ROS, lipid peroxide and GSH levels in B16-F10 cells. (A) CLSM image of intracellular ROS of B16-F10 cells after incubation with DOX, LipoFe and LipoDSSSD. Scale bar represents 100 μm. (B) CLSM image of intracellular lipid peroxide of B16-F10 cells treated with DOX, LipoFe and LipoDSSSD. The scale bar is 20 μm. (C-D) Flow cytometric analysis of intracellular ROS levels of B16-F10 cells treated with DOX, LipoFe and LipoDSSSD ($n = 3$, ***$P < 0.001$). (E) Intracellular GSH levels of B16-F10 cells treated with DOX, LipoFe and LipoDSSSD ($n = 3$, *$P < 0.05$).

the trisulfide linker by intracellular GSH allowed for drug release, and then drug migration to the nucleus for cell apoptosis.

3.3. *Intracellular ROS, lipid peroxide and GSH*

It is reported that iron could catalyze the generation of ROS for chemodynamic therapy [10,35]. We then evaluated the effect of these formulations on cellular ROS level in B16-F10 cells. As shown in Fig. 4A, 4C and 4D, DOX could slightly increase the fluorescence intensities of the DCF, which could be attributed to DOX-induced generation of H_2O_2 by up-regulation of the intracellular NOX4 [19]. In comparison, the ROS levels were significantly improved after treatment with LipoFe compared to that of the control group. It may benefit from iron redox couple mediated lipid peroxide [16]. In addition, Fe^{3+} containing LipoFe could be reduced to Fe^{2+} by intracellular GSH accompanied by the deplete of GSH (Fig. 4E). Then, the generated Fe^{2+} can react with the H_2O_2 in the tumor cells, and thus increasing the hydroxyl radical [16]. Combined the efficacy of LipoFe and DOX, cells treated with LipoDSSSD showed higher ROS levels compared to that of the LipoFe or DOX alone (Fig. 4A and 4D). The reaction of trisulfide-thiol exchange further contributed to GSH depletion and DOX release, inducing the generation of H_2O_2 to amplify Fenton-mediated ROS production (Fig. 4D and 4E). Therefore, LipoDSSSD induced the greatest amount of ROS generation and GSH depletion in tumor cells. Then, we sought to identify whether ferroptosis was involved in the therapy of LipoFe and LipoDSSSD. Lipid peroxide, as an important indicator of ferroptosis, was monitored by C11-BODIPY 581/591 probe [19]. As shown in Fig. 4B, iron and unsaturated lipids co-delivered LipoFe could induce obvious lipid peroxidation, in accordance with published literature [16]. Comparatively, the highest lipid peroxidation was observed for LipoDSSSD, where the released DOX would further amplify the ferroptosis effects of iron by producing H_2O_2.

3.4. *Pharmacokinetics and biodistribution*

We then tested the pharmacokinetic profiles of LipoDSSSD in comparison with free DOX in Sprague-Dawley rats. DOX had a poor circulation time, which was rapidly cleared from the body (Fig. 5A & 5B). In contrast, LipoDSSSD significantly improved the drug concentration in plasma, resulting in a longer circulation time compared to free DOX. Furthermore, most prodrugs remained intact, and only few DOX was released from DSSSD during systemic circulation. Owing to the low GSH in blood, LipoDSSSD reduced the undesired exposure of the free drug, which was consistent with the *in vitro* drug

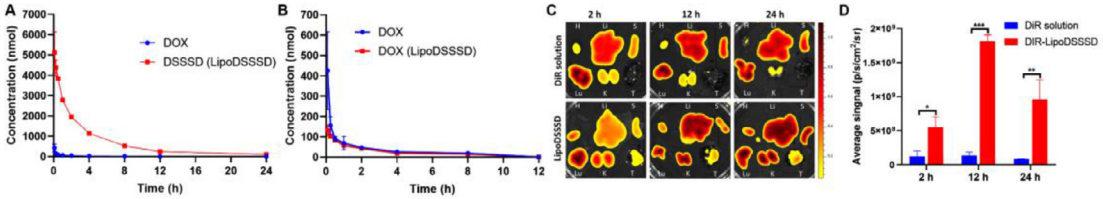

Fig. 5 – Pharmacometrics and biodistribution of LipoDSSSD. (A) Plasma concentration-time curves of DOX and the released DSSSD from LipoDSSSD. (B) Plasma concentration-time curves of DOX and the released DOX from LipoDSSSD. (C) Biodistribution of DiR solution and DiR labeled-liposome in B16-F10 melanoma-bearing mice. (D) Tumor accumulation of DiR solution and DiR labeled-liposome in tumor sites ($n = 3$, *$P < 0.05$, **$P < 0.01$, and ***$P < 0.001$).

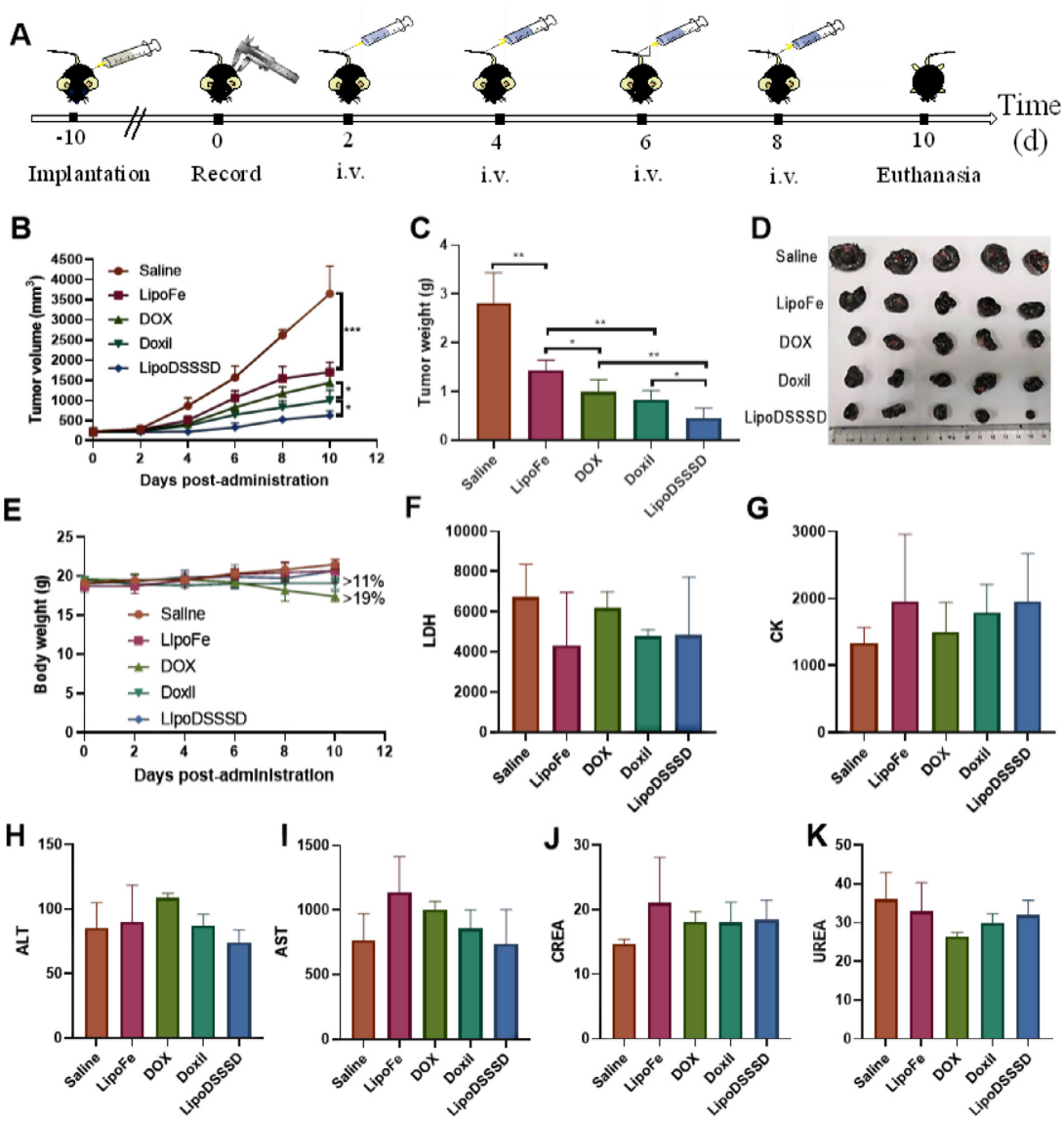

Fig. 6 – *In vivo* antitumor efficacy and safety. (A) Schedule for *in vivo* antitumor therapy. (B) Tumor growth curves and (C) tumor burden of B16-F10 melanoma-bearing mice during treatment with different formulations. (D) Images of B16-F10 tumors after receiving various treatments. (E) Body weight changes of B16-F10 melanoma-bearing mice during treatment with different formulations. Data are presented as means ± SD ($n = 5$, *$P < 0.05$, **$P < 0.01$, and ***$P < 0.001$). Hematological parameters after different treatments for (F) Lactate dehydrogenase (LDH; U/l), (G) Creatine kinase (CK; U/l), (H) Alanine aminotransferase (ALT; U/l), (I) Aspartate aminotransferase (AST; U/l), (J) Creatinine (CREA; μM/l) and (K) Urea nitrogen (UREA; mM/l). Data are presented as means ± SD ($n = 3$).

release in the absence of GSH. The detailed pharmacokinetic parameters of DOX and LipoDSSSD were summarized in Table S1. The area under the blood concentration curve (AUC) of LipoDSSSD was about 87-fold greater than that of the DOX solution after translation. We previously developed a DSSSD self-assembled nanomedicines, which suffered from undesired pharmacokinetics [23,28]. In comparison, LipoDSSSD integrated the advantages of prodrug and liposome, significantly reducing the undesired drug leakage but greatly prolonging the drug circulation.

The *in vivo* biodistribution was further investigated using fluorescent DiR labeled liposomes in B16-F10 melanoma tumor-bearing mice. As shown in Fig. 5C & 5D and Fig. S12, free DiR trended to accumulate in lungs rather than tumors. In comparison, a higher fluorescence accumulation was detected in tumors treated with liposomes, and the maximum fluorescent in tumors occurred at 12 h. The effective tumor accumulation of liposome could be attributed to the long blood-circulation and the EPR effect. Altogether, these results further confirmed the advantages of LipoDSSSD in terms of drug circulation and tumor accumulation.

3.5. *In vivo efficacy and safety*

The antitumor efficiency of LipoDSSSD was evaluated in B16-F10 melanoma tumor-bearing mice (Fig. 6A). LipoFe showed moderate tumor suppression in terms of tumor volume and tumor weight than that of saline group (Fig. 6B&D). The antitumor effect of LipoFe could be ascribed to Fenton-independent ferroptosis and inefficient Fenton-dependent ferroptosis. Liposomal Doxil showed a slightly stronger antitumor activity than DOX solution, indicating the improved therapy of liposomes, in accordance with previous studies [21]. However, obvious loss of body weight of B16-F10 melanoma-bearing mice was observed after treatment with Doxil (>11%) as well as free DOX (>19%) (Fig. 6E). This could be attributed to poor tolerance resulted from repeated dose toxicity of Doxil and free DOX. As an FDA-approved liposomal DOX formulation, Doxil could lower the risk of cardiotoxicity and myelosuppression of DOX, while inducing other dose-dependent adverse effect [21]. Comparatively, LipoDSSSD exhibited most significant tumor inhibition because of the combination of LipoFe-induced efficient ferroptosis and DOX-mediated apoptosis (Fig. 6B&D). Hematoxylin and eosin (H&E) staining and TUNEL staining further demonstrated the treatment with LipoDSSSD resulted in the highest level of apoptosis in tumor tissues (Fig. S13). Moreover, no distinct fluctuation was observed in terms of the body weight (Fig. 6E), the hematological parameters (Fig. 6F, & 6K), H&E staining of major organs (Fig. S14) of B16-F10 tumor bearing-mice after treatment with LipoDSSSD. These results demonstrated that LipoDSSSD exhibited potent antitumor activity but were well tolerated.

4. Conclusion

In summary, GSH-sensitive DSSSD was loaded into the lipid peroxide nanogenerator by the form of coordinate complex between DSSSD and iron via a novel Fe^{3+} gradient method. The developed LipoDSSSD integrated the advantage of liposomal drug delivery system and prodrug strategy. Consequently, liposomes prolonged the blood circulation of prodrugs while smart prodrugs relieved the adverse toxicity resulted from the elevated accumulation of liposomes. Furthermore, the Fe^{3+} could be efficiently reduced into Fe^{2+} under high GSH level in tumors, and subsequently catalyzed unsaturated lipids into lipid peroxidation for ferroptosis. The trisulfide bond of DSSSD could exchange with the overproduced GSH in tumor cells, enabling efficient GSH depletion and smart drug release, where DOX induced the generation of H_2O_2 to amplify the Fe^{2+}-mediated ferroptosis. This nanomedicine integrating ferroptosis and apoptosis dual treatment may be beneficial to the future cancer therapy.

Conflicts of interest

The authors declare no conflicts of interest.

Acknowledgments

This work was financially supported by the National Natural Science Foundation of China (no. 81872816), the Liaoning Revitalization Talents Program (no. XLYC180801). China Postdoctoral Innovative Talents Support Program (no. BX20190219) and China Postdoctoral Science Foundation (no. 2019M661134).

Supplementary materials

Supplementary material associated with this article can be found, in the online version, at doi:10.1016/j.ajps.2021.05.001.

REFERENCES

[1] Siegel RL, Miller KD, Jemal A. Cancer statistics, 2020. CA Cancer J Clin 2020;70(1):7–30.
[2] Shi J, Kantoff PW, Wooster R, Farokhzad OC. Cancer nanomedicine: progress, challenges and opportunities. Nat Rev Cancer 2017;17(1):20–37.
[3] van der Meel R, Sulheim E, Shi Y, Kiessling F, Mulder WJM, Lammers T. Smart cancer nanomedicine. Nat Nanotechnol 2019;14(11):1007–17.
[4] Bocci G, Kerbel RS. Pharmacokinetics of metronomic chemotherapy: a neglected but crucial aspect. Nat Rev Clin Oncol 2016;13(11):659–73.
[5] Jia D, Ma X, Lu Y, Li X, Hou S, Gao Y, et al. ROS-responsive cyclodextrin nanoplatform for combined photodynamic therapy and chemotherapy of cancer. Chin Chem Lett 2021;32(1):162–7.
[6] Bai S, Jia D, Ma X, Liang M, Xue P, Kang Y, et al. Cylindrical polymer brushes-anisotropic unimolecular micelle drug delivery system for enhancing the effectiveness of chemotherapy. Bioact Mater 2021;6(9):2894–904.
[7] Dixon SJ, Lemberg KM, Lamprecht MR, Skouta R, Zaitsev EM, Gleason CE, et al. Ferroptosis: an iron-dependent form of nonapoptotic cell death. Cell 2012;149(5):1060–72.
[8] Friedmann Angeli JP, Krysko DV, Conrad M. Ferroptosis at

the crossroads of cancer-acquired drug resistance and immune evasion. Nat Rev Cancer 2019;19(7):405–14.
[9] Hassannia B, Vandenabeele P, Vanden Berghe T. Targeting ferroptosis to iron out cancer. Cancer Cell 2019;35(6):830–49.
[10] Liu X, Jin Y, Liu T, Yang S, Zhou M, Wang W, et al. Iron-based theranostic nanoplatform for improving chemodynamic therapy of cancer. ACS Biomater Sci Eng 2020;6(9):4834–45.
[11] Liang C, Zhang X, Yang M, Dong X. Recent progress in ferroptosis inducers for cancer therapy. Adv Mater 2019;31(51):e1904197.
[12] Fu LH, Wan Y, Qi C, He J, Li C, Yang C, et al. Nanocatalytic theranostics with glutathione depletion and enhanced reactive oxygen species generation for efficient cancer therapy. Adv Mater 2021:e2006892.
[13] Foret MK, Lincoln R, Do Carmo S, Cuello AC, Cosa G. Connecting the "dots": from free radical lipid autoxidation to cell pathology and disease. Chem Rev 2020;120(23):12757–87.
[14] Yang WS, Kim KJ, Gaschler MM, Patel M, Shchepinov MS, Stockwell BR. Peroxidation of polyunsaturated fatty acids by lipoxygenases drives ferroptosis. Proc Natl Acad Sci USA 2016;113(34):E4966–75.
[15] Mozuraityte R, Rustad T, Storrø I. The role of iron in peroxidation of polyunsaturated fatty acids in liposomes. J Agric Food Chem 2008;56(2):537–43.
[16] He YJ, Liu XY, Xing L, Wan X, Chang X, Jiang HL. Fenton reaction-independent ferroptosis therapy via glutathione and iron redox couple sequentially triggered lipid peroxide generator. Biomaterials 2020;241:119911.
[17] Kosaraju SL, Tran C, Lawrence A. Liposomal delivery systems for encapsulation of ferrous sulfate: preparation and characterization. J Liposome Res 2006;16(4):347–58.
[18] Ma B, Wang S, Liu F, Zhang S, Duan J, Li Z, et al. Self-assembled copper-amino acid nanoparticles for *in situ* glutathione "AND" H_2O_2 sequentially triggered chemodynamic therapy. J Am Chem Soc 2019;141(2):849–57.
[19] Xue CC, Li MH, Zhao Y, Zhou J, Hu Y, Cai KY, et al. Tumor microenvironment-activatable Fe-doxorubicin preloaded amorphous $CaCO_3$ nanoformulation triggers ferroptosis in target tumor cells. Sci Adv 2020;6:eaax1346.
[20] Cagel M, Grotz E, Bernabeu E, Moretton MA, Chiappetta DA. Doxorubicin: nanotechnological overviews from bench to bedside. Drug Discov Today 2017;22(2):270–81.
[21] Barenholz Y. Doxil(R)–the first FDA-approved nano-drug: lessons learned. J Control Release 2012;160(2):117–34.
[22] Zhao N, Woodle MC, Mixson AJ. Advances in delivery systems for doxorubicin. J Nanomed Nanotechnol 2018;9(5):519.
[23] Yu J, Wang Y, Zhou S, Li J, Wang J, Chi D, et al. Remote loading paclitaxel-doxorubicin prodrug into liposomes for cancer combination therapy. Acta Pharm Sin B 2020;10(9):1730–40.
[24] Wei Y, Song S, Duan N, Wang F, Wang Y, Yang Y, et al. MT1-MMP-activated liposomes to improve tumor blood perfusion and drug delivery for enhanced pancreatic cancer therapy. Adv Sci 2020;7(17):1902746.
[25] Taresco V, Alexander C, Singh N, Pearce AK. Stimuli-responsive prodrug chemistries for drug delivery. Adv Therap 2018;1(4):1800030.
[26] Zhang X, Zhang T, Ma X, Wang Y, Lu Y, Jia D, et al. The design and synthesis of dextran-doxorubicin prodrug-based pH-sensitive drug delivery system for improving chemotherapy efficacy. Asian J Pharm Sci 2020;15(5):605–16.
[27] Sun X, Liu D, Xu X, Shen Y, Huang Y, Zeng Z, et al. NIR-triggered thermo-responsive biodegradable hydrogel with combination of photothermal and thermodynamic therapy for hypoxic tumor. Asian J Pharm Sci 2020;15(6):713–27.
[28] Yang Y, Sun B, Zuo S, Li X, Zhou S, Li L, et al. Trisulfide bond–mediated doxorubicin dimeric prodrug nanoassemblies with high drug loading, high self-assembly stability, and high tumor selectivity. Sci Adv 2020;6(45):eabc1725.
[29] Zuo S, Sun B, Yang Y, Zhou S, Zhang Y, Guo M, et al. Probing the superiority of diselenium bond on docetaxel dimeric prodrug nanoassemblies: small roles taking big responsibilities. Small 2020;16(45):2005039.
[30] Li L, Zuo S, Dong F, Liu T, Gao Y, Yang Y, et al. Small changes in the length of diselenide bond-containing linkages exert great influences on the antitumor activity of docetaxel homodimeric prodrug nanoassemblies. Asian J Pharm Sci 2021. doi:10.1016/j.ajps.2021.02.002.
[31] Kamoun WS, Kirpotin DB, Huang ZR, Tipparaju SK, Noble CO, Hayes ME, et al. Antitumour activity and tolerability of an EphA2-targeted nanotherapeutic in multiple mouse models. Nat Biomed Eng 2019;3(4):264–80.
[32] Shaikh IM, Tan KB, Chaudhury A, Liu Y, Tan BJ, Tan BMJ, et al. Liposome co-encapsulation of synergistic combination of irinotecan and doxorubicin for the treatment of intraperitoneally grown ovarian tumor xenograft. J Control Release 2013;172(3):852–61.
[33] Bacellar IOL, Oliveira MC, Dantas LS, Costa EB, Junqueira HC, Martins WK, et al. Photosensitized membrane permeabilization requires contact-dependent reactions between photosensitizer and lipids. J Am Chem Soc 2018;140(30):9606–15.
[34] Santra S, Kaittanis C, Santiesteban OJ, Perez JM. Cell-specific, activatable, and theranostic prodrug for dual-targeted cancer imaging and therapy. J Am Chem Soc 2011;133(41):16680–8.
[35] Yang B, Shi J. Ascorbate tumor chemotherapy by an iron-engineered nanomedicine-catalyzed tumor-specific pro-oxidation. J Am Chem Soc 2020;142(52):21775–85.